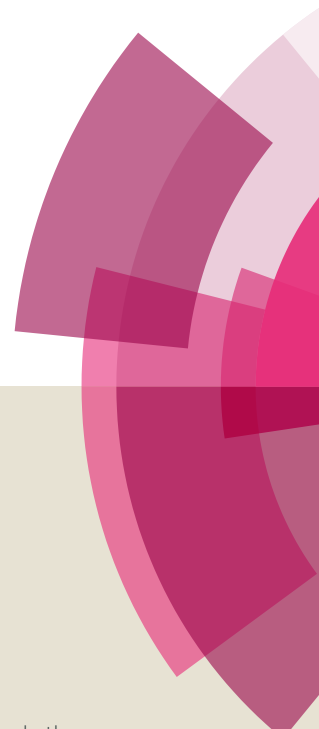


# NJC

Accepted Manuscript



This article can be cited before page numbers have been issued, to do this please use: Y. Xing, D. Li, B. Dong, X. Wang, C. Wu, L. Ding, S. Zhou, J. Fan and B. Song, *New J. Chem.*, 2019, DOI: 10.1039/C9NJ01184F.



This is an Accepted Manuscript, which has been through the Royal Society of Chemistry peer review process and has been accepted for publication.

Accepted Manuscripts are published online shortly after acceptance, before technical editing, formatting and proof reading. Using this free service, authors can make their results available to the community, in citable form, before we publish the edited article. We will replace this Accepted Manuscript with the edited and formatted Advance Article as soon as it is available.

You can find more information about Accepted Manuscripts in the [author guidelines](#).

Please note that technical editing may introduce minor changes to the text and/or graphics, which may alter content. The journal's standard [Terms & Conditions](#) and the ethical guidelines, outlined in our [author and reviewer resource centre](#), still apply. In no event shall the Royal Society of Chemistry be held responsible for any errors or omissions in this Accepted Manuscript or any consequences arising from the use of any information it contains.

Journal Name

ARTICLE

## Water-soluble and highly emissive near-infrared nano-probes by co-assembly of ionic amphiphiles: towards application in cell imaging

Yuzhi Xing<sup>a</sup>, Dahua Li<sup>a</sup>, Bin Dong<sup>a</sup>, Xiaocheng Wang<sup>a</sup>, Chengfeng Wu<sup>a</sup>, Lan Ding<sup>a</sup>, Shixin Zhou<sup>b,\*</sup>, Jian Fan<sup>c</sup> and Bo Song<sup>a,\*</sup>

Received 00th January 20xx,  
Accepted 00th January 20xx

DOI: 10.1039/x0xx00000x

www.rsc.org/

Water-soluble near-infrared (NIR) fluorescent dyes are extremely valuable in cell imaging. We here designed and synthesized an amphiphilic fluorescent dye (denoted by PBI-TPE-11), a bolaamphiphile bearing a conjugation of tetraphenylethylene and perylene bisimide in the middle and two aliphatic pyridinium at both ends. PBI-TPE-11 self-assembled into flake-like nanostructures in aqueous solution, and showed very weak fluorescent emission from 600 to 830 nm, covering the NIR region. This result seems discrepant with that previously reported in the literature, where the conjugation of PBI and TPE was proven an aggregation induced emission enhancing agent. Very interestingly, both the morphology and the emission intensity were altered by addition of sodium dodecyl benzene sulfonate (SDBS). Co-assembly of PBI-TPE-11 and SDBS formed nanowires, observed by atomic force microscope. Moreover, the emission of the co-assemblies was much stronger than the assemblies of neat PBI-TPE-11. An exciting quantum yield (QY) of 15% was obtained for the co-assemblies, while pure PBI-TPE-11 showed a QY of merely 0.2%. Finally, the co-assemblies were successfully applied in labeling the HeLa cells, and high viability and high contrast fluorescent images were achieved.

### Introduction

The development of near-infrared (NIR) fluorescence imaging is expected to have a significant impact on future personalized oncology owing to the low tissue autofluorescence and high tissue penetration depth in the NIR spectrum window (650 - 900 nm).<sup>1-3</sup> To date, a variety of materials have been extensively investigated for NIR fluorescence imaging, including fluorescent proteins<sup>4, 5</sup>, inorganic quantum dots<sup>6, 7</sup> and organic molecules<sup>8, 9</sup>. However, fluorescent proteins have some intrinsic disadvantages, for instance, small Stokes shift, poor photostability and tedious transfection process.<sup>10</sup> Inorganic quantum dots exhibit excellent emission property, but suffer from the high cytotoxicity resulting from heavy-metal elements (e.g. Cd & Se), especially in an oxidative environment.<sup>11</sup> In contrast, organic dyes have shown promising clinical applications as non-targeting agents for optical imaging because of its versatility and flexibility.<sup>12-15</sup>

The currently available organic NIR dyes include cyanine<sup>16</sup>, squaraine<sup>17</sup>, phthalocyanines<sup>18</sup>, porphyrin derivatives<sup>19, 20</sup> and borondipyrromethane (BODIPY) analogues<sup>21, 22</sup>. These dyes have their respective advantages, but also possess their own disadvantages, such as poor photostability, low quantum

yield and high plasma protein binding rate and so on.<sup>13, 14, 23, 24</sup> All in all, the molecular level dyes normally have strong intermolecular  $\pi$ - $\pi$  stacking interactions, and thus causes unpredictable nonradiative decay and consequently deficient fluorescence emission.<sup>25-27</sup> Such effect would be severely problematic in practical applications, especially in cell / tissue imaging. Therefore, fluorescent probes with high emission, water-solubility, low cytotoxicity and good stability are highly demanded for fluorescent bio-labeling.<sup>28</sup>

The fluorescence of organic dyes is prone to change depending on the outer environment, molecular configuration and aggregation state.<sup>29-32</sup> This feature acts as a double-edged sword in practical applications. In 1970s, acridine orange and pyrene have been used as probes to determine the critical micelle concentration, both of which utilized the environment dependent feature of the fluorescent dyes.<sup>33, 34</sup> Diarylethene and spiropyran both undergo isomerization upon irradiation, and their fluorescence changes with the configuration.<sup>35-37</sup> Nowadays, the popular aggregation induced emission (AIE) dyes demonstrate a very good example of fluorescence change with aggregation state.<sup>38, 39</sup> The fluorescence of organic dyes though vulnerable can be controlled by molecular interactions (inter or intra or both).

This research focuses on the fluorescent probes that are applicable in bio-systems. Therefore, water solubility (or dispersity) will be an extremely important character for the probes.<sup>40, 41</sup> Molecular assembly or co-assembly has proven to be a powerful tool for dealing with the supramolecular

<sup>a</sup> College of Chemistry, Chemical Engineering and Materials Science, Soochow University, Suzhou 215123, China. E-mail: songbo@suda.edu.cn

<sup>b</sup> Department of Cell Biology, School of Basic Medical Science, Peking University Health Science Center, Beijing 100191, China. E-mail: zsx@bjmu.edu.cn

<sup>c</sup> Jiangsu Key Laboratory For Carbon-Based Functional Materials & Devices Science, Soochow University, Suzhou 215123, China.

\* Electronic Supplementary Information (ESI) available.

See DOI: 10.1039/x0xx00000x

ARTICLE

Journal Name

interactions, especially the latter. Taking the advantage of coulombic interaction, co-assembly of amphiphiles with opposite charges has been widely investigated.<sup>42,43</sup> The idea has been employed to control the emission of dyes, mainly by tuning the interactions between the fluorescent moieties in the assemblies. For example, Benzhong Tang *et al.* synthesized a 2-(2-hydroxyphenyl)benzothiazole derivative with cationic groups to effectively detect the anionic surfactants, and the complex with enhanced emission was applied for bacterial imaging.<sup>44</sup> Yilin Wang *et al.* systematically investigated the surfactant types on the emission enhancing effect of cationic M-silole molecules.<sup>45</sup> Based on surfactant aggregate encapsulating, Liping Ding *et al.* developed a series of fluorescent sensors.<sup>46-48</sup> Deqing Zhang *et al.* designed a multi reaction system based on coulombic interactions, and developed a fluorescent “turn-on” method to detect the acetylcholinesterase.<sup>49</sup> Along with this idea, they also developed fluorometric “turn-on” detection of lactic acid and oxidase B.<sup>50, 51</sup> All these studies demonstrated that the co-assembly of amphiphiles bearing opposite charges should be a good avenue to control the fluorescence, especially for the AIE dyes. We are extremely interested in NIR dyes, and wonder if the co-assembly idea also works on them.

Perylene bisimides (PBIs) are one of the mostly investigated organic dyes with excellent photophysical, thermal and chemical stability.<sup>52-54</sup> Benzhong Tang *et al.* demonstrated that the conjugation of PBI and tetraphenylethylene (TPE) allows for AIE features and NIR emission to the resulting dye.<sup>55-57</sup> Inspired by their work, we attempt to introduce the jointed PBI and TPE into bolaamphiphile, and anticipate the self-assembled structures bring about efficient NIR emission that is applicable in cell imaging. The target molecule denoted by PBI-TPE-11 was hence synthesized. This molecule indeed showed a NIR emission ranging from 600-830 nm, however, the quantum yield was merely 0.2%. Employing the idea of co-assembly, we introduced anionic amphiphile sodium dodecyl benzene sulfonate (SDBS) in the aqueous solution of PBI-TPE-11. The co-assemblies kept the position of NIR emission, but the emission was significantly enhanced, and the quantum yield was promoted up to 15%. The co-assembly was proven a rather low cytotoxicity, and successfully applied in fluorescent imaging of HeLa cells.

Result and Discussion

The synthetic route of PBI-TPE-11 is shown in Fig. 1. Briefly, synthesis of trimethyl(4-(1,2,2-triphenylvinyl)phenyl)stannane (compound B) referred to literatures,<sup>58</sup> and it was prepared by reaction of compound A and n-butyl lithium. 11-bromoundecan-1-amine was synthesized according to the literatures.<sup>59</sup> Compound J was prepared by Stille coupling between compound B and alkylated PBI (compound H). The target molecule PBI-TPE-11 was characterized by NMR (Fig. S9) and mass spectra (Fig. S10). The detailed description of the synthesis is shown in the experimental section, and the corresponding characterization is shown in the supporting information.

Although the target molecule contains two pyridinium groups to improve the hydrophilicity, PBI-TPE-11 still shows a

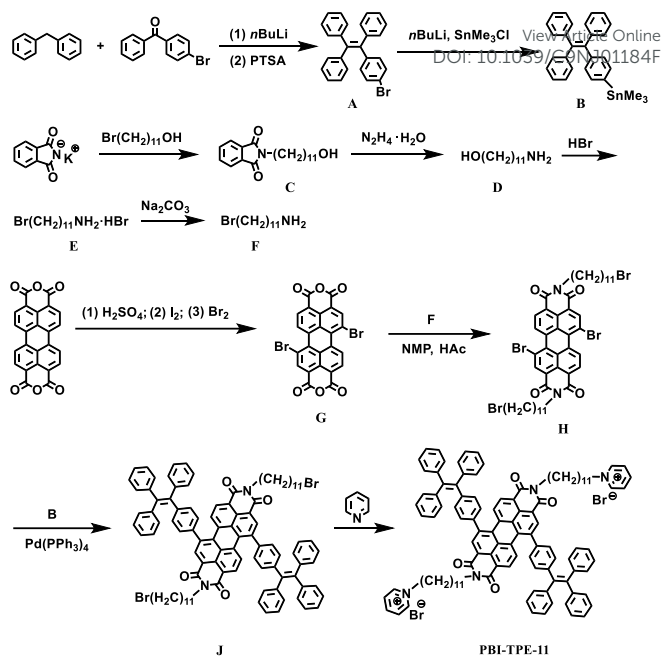
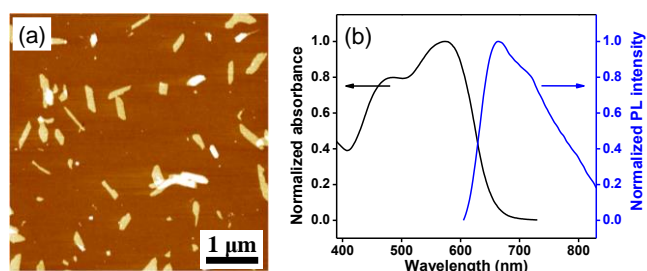


Fig. 1 The synthetic route of PBI-TPE-11

rather poor water solubility, which should be attributed to the combination of the hydrophobicity supplied by the alkyl chains and the strong  $\pi$ - $\pi$  stacking interactions between perylene groups. Methanol, a good solvent for PBI-TPE-11, was employed to assist PBI-TPE-11 dissolving in water. In doing so, PBI-TPE-11 was firstly dissolved in methanol (2% by volume to water), and then the solution was dropwise added into water. By this method, PBI-TPE-11 can be well dispersed in water. The concentration of PBI-TPE-11 was kept  $1.0 \times 10^{-5}$  mol L<sup>-1</sup> all through the research.

Firstly, the morphologies of the self-assembled structure were investigated by atomic force microscope (AFM). As shown in Fig. 2a, PBI-TPE-11 formed flake-like nanostructures in aqueous solution. Transmission electron microscope (TEM) observation also showed similar 2D structures, as shown in Fig. S11. The length of the lamellar structures is mostly in the range of 600-800 nm, and the width is in the range of 150-350 nm. The average thickness determined by the depth analysis was approximately 2.6 nm, as shown in Fig. S12. This value is less than the distance between the two pyridinium groups of extended PBI-TPE-11 molecule (4.4 nm, estimated by ChemDraw software). These results suggest that the lamellar structures should be composed of a single layer of PBI-TPE-11 molecules parallel packed at an inclined angle. This assumption should be reasonable that the hydrophilic pyridinium groups locate at the surfaces of the lamella, and the hydrophobic aromatic parts pack in order due to the intermolecular  $\pi$ - $\pi$  stacking interactions.

The absorption of PBI-TPE-11 ranges from 200-700 nm, and shows two peaks at 480 and 575 nm. In aqueous solution, it showed a rather weak fluorescence, which can be reflected by both the fluorescence intensity and the quantum yield. As shown in Fig. 1b, PBI-TPE-11 in aqueous solution displays an emission in the NIR region (600 - 830 nm, due to the detection



**Fig. 2** (a) The AFM image of PBI-TPE-11. (b) Normalized UV-vis and PL spectra of PBI-TPE-11 in aqueous solution.

limit of the instrument, we did not show the longer wavelength emission than 830 nm), and the peak position appears at 660 nm. The Stokes shift is approximately 90 nm. And the corresponding quantum yield is 0.2%, determined by relative method using cresyl violet as reference.

Upon addition of 2-fold SDBS, the lamellar structures were no longer observed but replaced by discrete nanowires in the AFM image, as shown in Fig. 3a. The width of the nanowires is in the range of 50-200 nm, and the average thickness is almost unchanged compared with the nano-flakes formed by PBI-TPE-11 (Fig. S12). The morphological change indicates that the SDBS should have some kind of interaction with PBI-TPE-11, and the bonding between them altered the assembled structure.

We were happy to find that the fluorescence was significantly enhanced upon addition of 2-fold SDBS into the PBI-TPE-11 solution. As shown in Fig. 3b, the fluorescence intensity became 12 times of the assemblies formed by neat PBI-TPE-11, and the quantum yield increased to 2%. Such fluorescence enhancement could be observed by naked eyes under illumination of 365 nm UV light (inset in Fig. 3b). Moreover, the quantum yield continues to increase when adding more SDBS, and a quantum yield as high as 15% was acquired when 140-fold of SDBS was added. It is worth to note that the critical aggregation concentration (CMC) of SDBS is  $1.6 \times 10^{-3} \text{ mol L}^{-1}$ .<sup>60, 61</sup> Herein, the SDBS added into the aqueous solution of PBI-TPE-11 was still less than its CMC, which means that the fluorescence change should be attributed to the formation of complexes between PBI-TPE-11 and SDBS mainly relying on two supramolecular interactions: (1) the electrostatic interaction between the ionic head groups of the PBI-TPE-11 and SDBS, (2) the hydrophobic interaction supplied by the aliphatic chains.

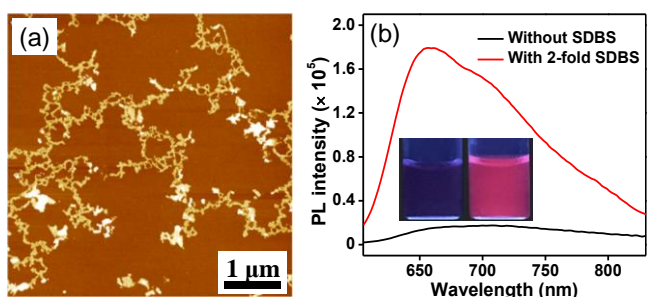


**Fig. 3** (a) The AFM image of PBI-TPE-11 in presence of 2-fold SDBS. (b) Fluorescence spectra of PBI-TPE-11 in absence and presence of 2-fold SDBS in aqueous solution ( $\lambda_{\text{ex}} = 585 \text{ nm}$ ). Inset: Photographs of the corresponding solution under illumination of 365 nm UV light.

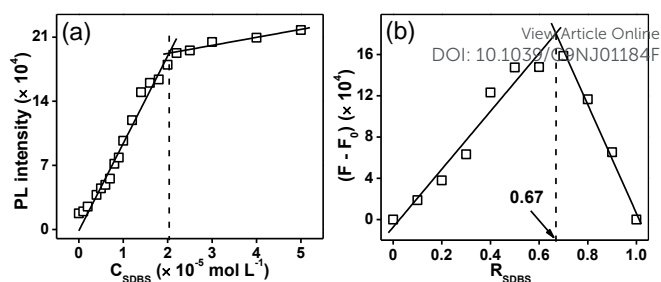


**Fig. 4** (a) Plot of fluorescence intensity at 660 nm versus  $C_{\text{SDBS}}$ . (b) Job's plot.

The co-assembly of PBI-TPE-11/SDBS was also confirmed by zeta potential measurement. The zeta potential of the assemblies of PBI-TPE-11 and co-assemblies of PBI-TPE-11/SDBS were  $35.6 \pm 2.6$  and  $-42.3 \pm 2 \text{ mV}$ , respectively. PBI-TPE-11 and SDBS are cationic and anionic amphiphiles, respectively. Based on this result, it is understandable that the zeta potentials of the particles turn from positive to negative after co-assembly. In addition, the suspension of the co-assemblies of PBI-TPE-11/SDBS kept clear and showed no precipitation for at least 7 days (Fig. S13), indicating that it should be a true colloidal solution.

Secondly, the association ratio between PBI-TPE-11 and SDBS was determined by two methods. (1) As aforementioned, increasing SDBS in the aqueous solution of PBI-TPE-11 will lead to the enhancement of the fluorescence. This feature was utilized to estimate the association ratio. In doing so, the concentration of PBI-TPE-11 was kept constant at  $1.0 \times 10^{-5} \text{ mol L}^{-1}$ , and the concentration of SDBS ( $C_{\text{SDBS}}$ ) was varied. The fluorescence intensity at the 660 nm (the peak position) was plotted against the corresponding concentration. As shown in Fig. 4a, linear fitting presented a slope change at the concentration of  $2.0 \times 10^{-5} \text{ mol L}^{-1}$ , which implies that the association ratio between PBI-TPE-11 and SDBS should be 1:2. An equilibrium must be existed between these two compounds and their complexes. Passing the association ratio point, the increase of fluorescence relies on the amount of extra SDBS to push the equilibrium to right side, which makes a reasonable explanation for the smaller slope. (2) The second method used to determine the association ratio was Job's plot.<sup>62</sup> In doing so, the total concentration of these two compounds was kept constant ( $1.0 \times 10^{-4} \text{ mol L}^{-1}$ ), and the molar ratios of SDBS ( $R_{\text{SDBS}}$ ) were varied from 0 to 1. The fluorescence differences ( $F - F_0$ , where  $F$  and  $F_0$  are the fluorescence intensity in presence and absence of SDBS respectively) were plotted against  $R_{\text{SDBS}}$ . As shown in Fig. 4b, a maximum emission was obtained as  $R_{\text{SDBS}} = 0.67$  by linear fitting, which confirms that the association ratio of PBI-TPE-11 and SDBS is 1:2.

Since we have learned that the association ratio between PBI-TPE-11 and SDBS is 1:2, the association constant of the complex can be determined by Benesi-Hildebrand equation<sup>63, 64</sup>:

$$\frac{1}{F - F_0} = \frac{1}{K_a \cdot (F_{\text{max}} - F_0) \cdot C_{\text{SDBS}}^2} + \frac{1}{F_{\text{max}} - F_0}$$

where  $F_{\text{max}}$  is the maximum fluorescence intensity of PBI-TPE-11 in presence of SDBS,  $K_a$  is the association constant. As shown

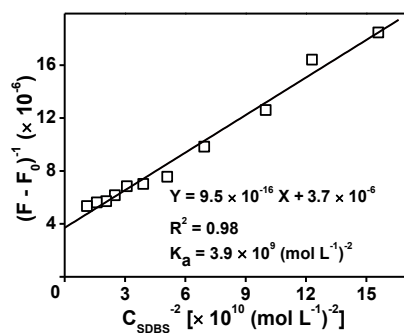


Fig. 5 Benesi-Hildebrand's plot of  $(F - F_0)^{-1}$  versus  $C_{\text{SDBS}}^{-2}$ .

in Fig. 5,  $K_a$  was extrapolated by linear fitting of the plot of  $(F - F_0)^{-1}$  against  $C_{\text{SDBS}}^{-2}$ , and the value was  $3.9 \times 10^9 \text{ (mol L}^{-1}\text{)}^{-2}$ , indicating that PBI-TPE-11 have very high affinity with SDBS. The high affinity should be attributed to electrostatic interaction between the pyridinium head of PBI-TPE-11 and the sulfonate group of SDBS.

Thirdly, the complexation between PBI-TPE-11 and SDBS can also be qualitatively analyzed through Fourier transform infrared (FTIR) spectroscopy, and the spectra are shown in Fig. 6. As for the neat PBI-TPE-11, the distinct vibration peaks at 1695, 1658 and 1635  $\text{cm}^{-1}$  are assigned to the stretching vibration of carbonyl bonds in amide I, and peaks at 1597 and 1587  $\text{cm}^{-1}$  are due to the stretching vibration of C=C in perylene.<sup>65</sup> Upon addition of SDBS, the peak located at 1695  $\text{cm}^{-1}$  became very weak, and a new peak appears at 1733  $\text{cm}^{-1}$ . This alteration could be explained by reduced interaction between the perylene bisimide due to the intercalation of SDBS. The conjugate delocalization effect owing to the strong  $\pi$ - $\pi$  stacking interaction will decrease the polarity of carbonyl group, and hence results in a relatively low wavenumber vibration at 1695  $\text{cm}^{-1}$ . The segregation effect induced by intercalation of SDBS will decrease the  $\pi$ - $\pi$  stacking interaction, and thus the typical vibration peak (1733  $\text{cm}^{-1}$ ) of isolated carbonyl groups appeared. The above assumption can also explain the disappeared peak at 1597 and 1587  $\text{cm}^{-1}$ . Due to the reduced  $\pi$ - $\pi$  stacking interaction, the vibration of C=C shifted to normal position at around 1600  $\text{cm}^{-1}$ . These results accord with the morphology change, as well as the greatly enhanced fluorescence emission.

Based on the above experiment facts, we can conclude that the fluorescence enhancement of PBI-TPE-11 upon addition of

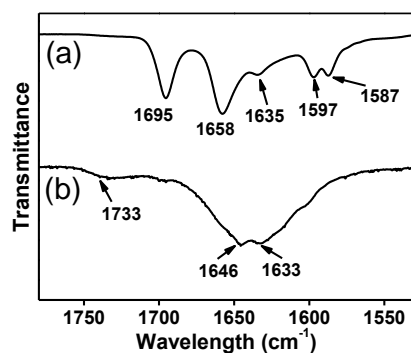


Fig. 6 FTIR spectra of (a) PBI-TPE-11; (b) complex of PBI-TPE-11 with SDBS.

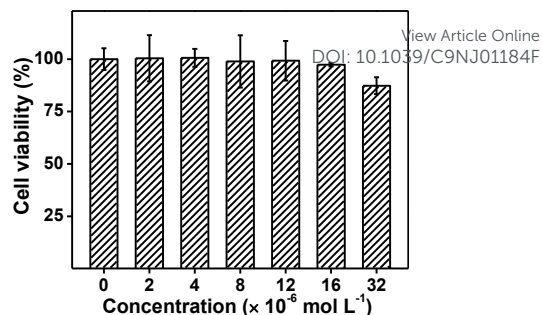
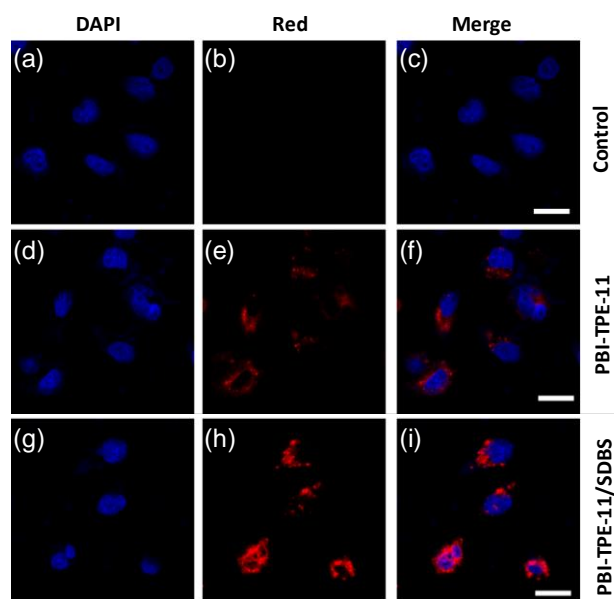


Fig. 7 Dose-dependent cell viability of complex of PBI-TPE-11 and SDBS with HeLa cells.

SDBS should be attributed to the tailored intermolecular interactions. As for the neat PBI-TPE-11 in aqueous solution,  $\pi$ - $\pi$  stacking interactions caused by the planar perylene bisimide and hydrophobic interaction make the molecules pack in order. Co-assembly of PBI-TPE-11 and SDBS reduced the strong  $\pi$ - $\pi$  stacking interaction by the alkyl chains intercalating in between the perylene bisimide groups, and thus led to the enhanced fluorescence emission. When more than 2-fold SDBS was added, the extra SDBS molecules possibly segregated the PBI-TPE-11 molecules by surrounding them, which explains the continuous increase of quantum yield.

In the following, the cell viability was tested under existence of co-assemblies of PBI-TPE-11 and SDBS. As shown in Fig. 7, the viabilities of HeLa cells were almost 100% when the concentration of PBI-TPE-11 was lower than  $16 \times 10^{-6} \text{ mol L}^{-1}$ , and when the concentration was  $32 \times 10^{-6} \text{ mol L}^{-1}$ , the cell viability value was still maintained  $> 85\%$ . The concentration of PBI-TPE-11 used in cell imaging was much lower than  $16 \times 10^{-6} \text{ mol L}^{-1}$ , and hence the cytotoxicity is negligible.

The PBI-TPE-11 and co-assemblies of PBI-TPE-11/SDBS were applied to stain the HeLa cells. To locate the position of the complex, the HeLa cells were cultured in the mediums containing 4',6-diamidino-2-phenylindole (DAPI), PBI-TPE-11 and co-assemblies of PBI-TPE-11/SDBS. The concentration of PBI-TPE-11 in the culturing mediums was controlled to  $7 \times 10^{-6} \text{ mol L}^{-1}$ , which is far below the toxic dosage. To make a good comparison, the cells only labeled with DAPI and labeled with DAPI and PBI-TPE-11 were employed as the control. The HeLa cells were sequentially labeled by DAPI and the nano-probes by culturing them in the mediums containing these probes. After being fixed by polyaldehyde, the cells were observed by confocal laser scanning microscope (CLSM). It is worth to note that DAPI is often used to stain the nuclei of cells, and it emits strong blue fluorescence, whose brightness can be applied as reference to the rest. As shown in Fig. 8, the blue emission stands for the location of the nuclei, and the red emission is the fluorescence emission of nano-probes (assemblies of PBI-TPE-11 or co-assemblies of PBI-TPE-11/SDBS). It is clear that the co-assemblies resided in the cytoplasm of HeLa cells, and the nuclei were not stained by them. Besides, the cells labeled with PBI-TPE-11 showed weak fluorescent emission comparing to those labeled with the co-assemblies of PBI-TPE-11/SDBS. These data



**Fig. 8** CLSM images of HeLa cells after being cultured in the mediums: (a-c) without PBI-TPE-11, (d-f) with PBI-TPE-11, and (g-i) with co-assemblies of PBI-TPE-11/SDBS. From left to right rows are images of cells labeled with DAPI, PBI-TPE-11 (or PBI-TPE-11/SDBS), and merged images of the former two. Scale bar: 20  $\mu\text{m}$ .

indicate that the co-assemblies should be an excellent NIR nano-probe for cell imaging.

The photostability of the nano-probes is one of the most important concerns for bioimaging. We investigated the photostability of PBI-TPE-11/SDBS, and the results are shown in Fig. 9.  $F_0$  and  $F$  are the initial PL intensity and the PL intensity of the sample at different irradiation time. The PL intensity showed a little decrease after being continuously irradiated by 561 nm (2mW) light for 20 min, and the nano-probes possess  $\approx 92\%$  of their initial PL intensity, as shown in Fig. 9. In addition, the CLSM image did not show big differences on their contrast and resolution. These results indicate the nano-probes have excellent photostability.

## Conclusions

In summary, a bolaamphiphile bearing conjugation of PBI and TPE was synthesized. As being dispersed in aqueous solution, it showed a weak NIR fluorescence emission. Co-assembly of PBI-TPE-11 and SDBS greatly enhanced the fluorescence emission, and the quantum yield was promoted from 0.2% to 15%. It was proven that PBI-TPE-11 and SDBS have very strong association with a ratio of 1:2. The co-assemblies showed no toxicity until  $16 \times 10^{-6} \text{ mol L}^{-1}$ , and were demonstrated a very good NIR nano-emitter in cell imaging.

## Experimental

**Materials.** Diphenylmethane, 4-bromobenzophenone, *n*-butyl lithium, *p*-toluenesulfonic acid (PTSA), trimethylstannanylium chloride ( $\text{SnMe}_3\text{Cl}$ ) and cresyl violet were purchased from J&K Chemical Co., Ltd. (Shanghai). 11-Bromo-1-undecanol,

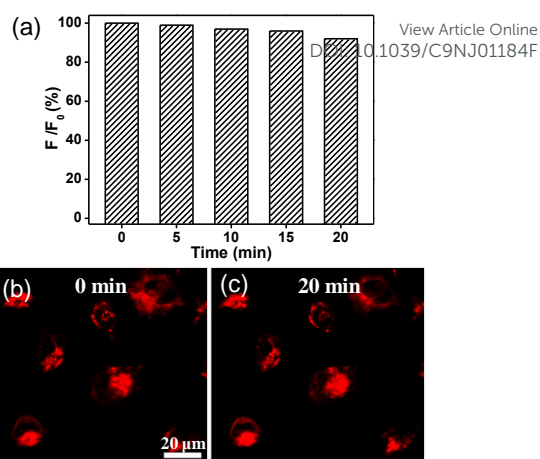


**Fig. 9** (a) Photostability test of PBI-TPE-11/SDBS in HeLa cells. The cells were continuously irradiated at 561 nm (2 mW) for 20 min, and the fluorescent intensities were recorded every 5 min. Two typical CLSM images of the cells labeled with the co-assemblies of PBI-TPE-11/SDBS are presented: (b) 0 min, (c) 20 min.

phthalimide potassium salt, hydrazine hydrate, HBr (48 wt.% solution in  $\text{H}_2\text{O}$ ), perylene-3,4,9,10-tetracarboxylic dianhydride,  $\text{Pd}(\text{PPh}_3)_4$  and sodium SDBS were purchased from TCI (Shanghai) Development Co., Ltd. Tetrahydrofuran (THF), toluene, *N,N*-dimethylformamide (DMF), methanol, ethanol, acetone, acetic acid, 1-methyl-2-pyrrolidone (NMP),  $\text{H}_2\text{SO}_4$  (98%), HCl, NaCl, NaOH, anhydrous  $\text{Na}_2\text{SO}_4$ , anhydrous  $\text{Na}_2\text{CO}_3$ , anhydrous  $\text{NH}_4\text{Cl}$ , iodine, bromine and pyridine were purchased from Sinopharm Chemical Reagent Co., Ltd. Ethyl acetate, petroleum ether, dichloromethane (DCM), and chloroform were obtained from Yonghua Chemical Technology (Jiangsu) Co., Ltd.

**Characterization.**  $^1\text{H}$  NMR spectra were recorded on a Bruker Avance III 400 MHz NMR spectrometer (USA). Mass spectra (MS) of compound 6 was obtained on a micro Q-TOF III mass spectrometer (Bruker, USA) in the electrospray ionization (ESI) mode. And other products were measured with matrix-assisted laser desorption/ionization time-of-flight (MALDI-TOF-MS). The measurements of the fluorescence spectra were conducted on FLS980 (Edinburgh Instrument). AFM images were recorded on a Multimode 8 microscope (Bruker, USA). Peak force quantitative nanomechanical mapping mode with a Scan Asyst-Air probe (nominal spring constants  $0.4 \text{ N m}^{-1}$ , frequency 70 kHz, from Bruker) was adopted during the measurement. The samples were cast on a silicon substrate and dried in vacuum, and the concentration of PBI-TPE-11 was  $1.0 \times 10^{-5} \text{ mol L}^{-1}$ . TEM characterization was performed on Hitachi HT7700 (Japan) operating at 120 kV. Approximately 10  $\mu\text{L}$  of sample solution was cast onto carbon-coated copper grid, and then the grid was dried under vacuum. FTIR spectra were recorded on a Nicolet 6700 produced by Thermo Scientific (USA). The cell images were taken on a STP6000 CLSM (LEICA, Germany).

**Synthesis of (2-(4-bromophenyl)ethene-1,1,2-triyl)tribenzene (compound A).** A 1.6 M solution of *n*-butyl lithium in hexane (2.6 mL, 4.16 mmol) was added dropwise to the solution of diphenylmethane (0.78 g, 4.7 mmol) in anhydrous THF (60 mL) at  $0^\circ\text{C}$  in a nitrogen atmosphere. After the mixture being stirred

for 30 min at 0 °C, 4-bromobenzophenone (1.0 g, 3.8 mmol) was added at -78 °C, and the mixture was continuously stirred for 5 h. Afterward, the reactant was allowed to warm to room temperature. Then, the reaction was quenched with aqueous solution of NH<sub>4</sub>Cl and extracted with DCM, and dried over anhydrous Na<sub>2</sub>SO<sub>4</sub>. After removal of the solvent by rotavapor, the crude product was dissolved in toluene (100 mL). Then PTSA (50 mg, 0.29 mmol) was added, and the mixture was refluxed for 2.5 h before cooling to room temperature. The solvent was removed and the crude product was purified by silica gel column chromatography using hexane/chloroform (30/1 by volume) as eluent. Yield: 0.6 g, 43%. <sup>1</sup>H NMR (400 MHz, CDCl<sub>3</sub>, δ): 7.22 (d, *J* = 8.0 Hz, 2H), 7.16-7.06 (m, 9H), 7.05-6.97 (m, 6H), 6.89 (d, *J* = 8.0 Hz, 2H).

**Synthesis of trimethyl(4-(1,2,2-triphenylvinyl)phenyl)stannane (compound B).** Compound A (2.0 g, 4.9 mmol) was added into anhydrous THF (60 mL) at -78 °C under nitrogen atmosphere, then a 1.6 M solution of *n*-butyl lithium in hexane (4.2 mL, 6.7 mmol) was dropped into it over 20 min. After stirring for 2 h, a 1.0 M solution of SnMe<sub>3</sub>Cl in hexane (8.8 mL, 8.8 mmol) was added and reacted for 12 h at room temperature. Then the mixture was poured into water and extracted with ethyl acetate. After removing the solvent, the crude product was obtained and used directly in the next synthesis.

**Synthesis of 2-(11-hydroxyundecyl)isoindoline-1,3-dione (compound C).** 11-Bromo-1-undecanol (5.0 g, 27.0 mmol) and phthalimide potassium salt (5.5 g, 22.0 mmol) were dissolved in DMF (150 mL), and the mixture was stirred at 80 °C for 18 h. After cooling down, the reactant was diluted with ethyl acetate. The organic layer was washed with water for three times. The collected water layer was extracted three times with ethyl acetate. The organic layer was washed with brine twice and dried over anhydrous Na<sub>2</sub>SO<sub>4</sub>. After removing the solvent, the crude product was recrystallized from methanol, and was used directly in the next synthesis.

**Synthesis of 11-aminoundecan-1-ol (compound D).** Hydrazine hydrate (4.0 mL, 82.4 mmol) was slowly added into the solution of compound C (6.0 g, 19.8 mmol) in ethanol (100 mL). The reactant was refluxed for 3 h. After cooling down, the reactant was adjusted to pH 1 with 4 M HCl, then filtered. The filtrate was extracted with DCM for three times. After the collected aqueous layer was adjusted to pH 14 with concentrated NaOH solution, it was extracted with DCM for five times. The organic phase was dried over anhydrous Na<sub>2</sub>SO<sub>4</sub>. After removing the solvent, the crude product was obtained and used directly in the next step.

**Synthesis of 11-bromoundecan-1-ammonium bromide (compound E).** Compound D (6 g, 32 mmol) and HBr (40 mL, 48 wt.% solution in H<sub>2</sub>O) were stirred at 100 °C for 24 h. After being cooled down, the precipitate was filtered and washed with water for three times. The crude product was recrystallized from acetone. Yield: 8.6 g, 82%. <sup>1</sup>H NMR (400 MHz, DMSO-*d*<sub>6</sub>, δ): 7.61 (s, 3H), 3.52 (t, *J* = 6.7 Hz, 2H), 2.81-2.68 (m, 2H), 1.84-1.70 (m, 2H), 1.53-1.44 (m, 2H), 1.41-1.18 (m, 14H).

**Synthesis of 11-bromoundecan-1-amine (compound F).** The aqueous solution (35 mL) of Na<sub>2</sub>CO<sub>3</sub> (3.4 g, 32.0 mmol) was added into solution of compound E (3.9 g, 11.8 mmol) in DCM (30 mL). The mixture was stirred at room temperature for 30 min. Then the resulting product was extracted with DCM, and dried over anhydrous Na<sub>2</sub>SO<sub>4</sub>. After the removal of solvent, the crude product was obtained and used directly in the next step. Yield: 2.9 g, 98%. <sup>1</sup>H NMR (400 MHz, CDCl<sub>3</sub>, δ): 3.40 (t, *J* = 6.9 Hz, 2H), 2.70 (t, *J* = 7.1 Hz, 2H), 1.89-1.80 (m, 2H), 1.43 (dd, *J* = 16.5, 7.6 Hz, 4H), 1.34-1.23 (m, 14H). ESI-MS (*m/z*): calcd for [C<sub>11</sub>H<sub>24</sub>BrN + H]<sup>+</sup>: 249.1165, found: 250.1195.

**Synthesis of 1,7-dibromo-3,4,9,10-tetracarboxylic perylene dianhydride (compound G).** Perylene-3,4,9,10-tetracarboxylic dianhydride (10.0 g, 25.5 mmol) and concentrated H<sub>2</sub>SO<sub>4</sub> (100 mL) were added into a 250 mL three-necked flask. The mixture was stirred at 55 °C for 18 h. Iodine (250 mg, 1.0 mmol) was added to the mixture, and continuously stirred for 5 h. Bromine (2.9 mL, 56.1 mmol) was added dropwise to the mixture over 30 min, then the reaction was stirred at 85 °C for 24 h. After cooling to 40 °C, the excess bromine was blown with nitrogen under stirring. Then the mixture was poured into ice-water, and the precipitate was separated by filtration. The precipitate was washed with water until the filtrate was neutral. The crude product was used without further purification.

**Synthesis of N,N'-undecyl-1,7-dibromo-3,4,9,10-tetracarboxylic perylene bisimide (compound H).** Compound G (3.2 g, 6.0 mmol) and NMP (90 mL) were added into a flask, and the mixture was sonicated for 30 min. Then compound F (4.0 g, 16.0 mmol) and acetic acid (15 mL) were added to the reaction mixture. The resulting solution was stirred at 85 °C for 48 h under nitrogen atmosphere. Afterward, the reaction solution was cooled to room temperature. Then, the mixture was poured into ice-water (500 mL). The precipitate was separated by filtration. The crude product was purified by a silica gel column chromatography using chloroform as eluent. Yield: 1.0 g, 17%. <sup>1</sup>H NMR (400 MHz, CDCl<sub>3</sub>, δ): 9.49 (d, *J* = 8.2 Hz, 2H), 8.93 (s, 2H), 8.71 (d, *J* = 8.1 Hz, 2H), 4.34-4.11 (m, 4H), 3.41 (t, *J* = 6.9 Hz, 4H), 1.89-1.80 (m, 4H), 1.80-1.70 (m, 4H), 1.47-1.21 (m, 28H). MALDI-TOF-MS (*m/z*): calcd for [C<sub>46</sub>H<sub>50</sub>Br<sub>2</sub>N<sub>2</sub>O<sub>4</sub> + H]<sup>+</sup>: 1015.054, found: 1015.067.

**Synthesis of N,N'-undecyl-1,7-di(4-(1,2,2-triphenylvinyl)phenyl)-3,4,9,10-tetracarboxylic perylene bisimide (compound J).** Compound H (445 mg, 0.9 mmol), compound B (300 mg, 0.3 mmol) and Pd(PPh<sub>3</sub>)<sub>4</sub> (35 mg, 0.03 mmol) were added into a two-necked flask. Under protection of argon, anhydrous toluene (100 mL) was added. The reactants were refluxed for 48 h. After removing the solvent, the product was purified by a silica gel column chromatography using DCM/petroleum ether (7/2 by volume) as eluent. Yield: 150 mg, 33%. <sup>1</sup>H NMR (400 MHz, CDCl<sub>3</sub>, δ): 8.61 (s, 2H), 8.23 (d, *J* = 8.2 Hz, 2H), 7.86 (d, *J* = 8.2 Hz, 2H), 7.37-7.09 (m, 38H), 4.33-4.20 (m, 4H), 3.44 (t, *J* = 6.9 Hz, 4H), 1.93-1.82 (m, 4H), 1.77 (dd, *J* = 15.7, 7.3 Hz, 4H), 1.55-1.28 (m, 28H). MALDI-TOF-MS (*m/z*): calcd for [C<sub>98</sub>H<sub>88</sub>Br<sub>2</sub>N<sub>2</sub>O<sub>4</sub> + H]<sup>+</sup>: 1517.518, found: 1517.515.

**Synthesis of PBI-TPE-11.** Compound J (150 mg, 0.1 mmol) was dissolved in pyridine (100 mL), and refluxed for 48 h. After removing the solvent, the product was washed with ethyl ether for five times. Yield: 120 mg, 72%.  $^1\text{H NMR}$  (400 MHz,  $\text{DMSO-}d_6$ ,  $\delta$ ): 9.13 (d,  $J = 4.7$  Hz, 4H), 8.60 (t,  $J = 7.6$  Hz, 2H), 8.15 (t,  $J = 6.5$  Hz, 4H), 8.02 (s, 2H), 7.54-7.45 (m, 2H), 7.41-6.79 (m, 40H), 4.60 (t,  $J = 7.0$  Hz, 4H), 4.18-3.91 (m, 4H), 1.97-1.82 (m, 4H), 1.73-1.54 (m, 4H), 1.42-1.14 (m, 28H). MALDI-TOF-MS ( $m/z$ ): calcd for  $[\text{C}_{108}\text{H}_{98}\text{Br}_2\text{N}_4\text{O}_4 - 2\text{Br}]^{2+}$ : 757.881, found: 757.859.

**Cell viability assay.** The cell viability of the complex formed by PBI-TPE-11 and SDBS on HeLa cells was evaluated by CCK-8 assay (Dojindo, Japan). The preparation of the HeLa cells and incubation of complexes were similar to those in the cell imaging process. After being cultivated for 12 h, HeLa cells were incubated with a series of concentrations of complexes (the concentrations of PBI-TPE-11 were 0, 2, 4, 8, 12, 16,  $32 \times 10^{-6}$  mol  $\text{L}^{-1}$ , mixed with 2-fold SDBS respectively). After 12 h of incubation of the HeLa cells, each well of the plate was added 10  $\mu\text{L}$  of CCK-8 solution and incubated for 2 h in the 37  $^\circ\text{C}$  incubator. The detection of absorbance at 450 nm was used a microplate reader (Spectramax i3, Molecular Devices, USA). And the absorbance values were proportional to the number of live cells. Each concentration had three parallel wells.

**Cell culture and imaging.** HeLa cells were cultivated in Dulbecco's Modified Eagle Medium (DMEM, ThermoFisher) medium supplemented with 10% fetal bovine serum (Hyclone). For cell imaging, the solution of complexes formed by PBI-TPE-11 and SDBS (the concentration of PBI-TPE-11 was about  $7 \times 10^{-6}$  mol  $\text{L}^{-1}$ , mixed with 2-fold SDBS) was added into a bottom-glass dish seeded with HeLa cells and incubated at 37  $^\circ\text{C}$  for 2 h. After that, the cells were gently washed twice with phosphate buffered saline (PBS) and fixed by 2% paraformaldehyde for 40 min. Lastly, nuclear DNA of the cells was stained with DAPI for 20 min at room temperature, and the cells were washed for 3 times with PBS buffer solution. Then the cells were imaged with CLSM.

## Conflicts of interest

There are no conflicts to declare.

## Acknowledgements

We thank the financial support of the National Nature Science Foundation of China (21674075 and 21233003), the Nature Science Foundation of Jiangsu Province (BK20161211), Key University Science Research Project of Jiangsu Province (17KJA150007), Suzhou Key Laboratory of Macromolecular Design and Precision Synthesis, Jiangsu Key Laboratory For Carbon-Based Functional Materials & Devices Science, State and Local Joint Engineering Laboratory for Novel Functional Polymeric Materials, and a Project Funded by the Priority Academic Program Development of Jiangsu Higher Education Institutions.

## Notes and references

View Article Online  
DOI: 10.1039/C9NJ01184F

- K.-Y. Pu, K. Li and B. Liu, *Adv. Funct. Mater.*, 2010, **20**, 2770-2777.
- C. Yang, H. Liu, Y. Zhang, Z. Xu, X. Wang, B. Cao and M. Wang, *Biomacromolecules*, 2016, **17**, 1673-1683.
- H. Chen, T. Liu, Z. Su, L. Shang and G. Wei, *Nanoscale Horizons*, 2018, **3**, 74-89.
- R. E. Campbell, O. Tour, A. E. Palmer, P. A. Steinbach, G. S. Baird, D. A. Zacharias and R. Y. Tsien, *Proc. Natl. Acad. Sci.*, 2002, **99**, 7877-7872.
- X. Shu, A. Royant, M. Z. Lin, T. A. Aguilera, V. Lev-Ram, P. A. Steinbach and R. Y. Tsien, *Science*, 2009, **324**, 804-807.
- Z. Lin, X. Fei, Q. Ma, X. Gao and X. Su, *New J. Chem.*, 2014, **38**, 90-96.
- X. Michalet, F. F. Pinaud, L. A. Bentolila, J. M. Tsay, S. Doose, J. J. Li, G. Sundaresan, A. M. Wu, S. S. Gambhir and S. Weiss, *Science*, 2005, **307**, 538-544.
- Y. Yang, M. Lowry, X. Xu, J. O. Escobedo, M. Sibrían-Vazquez, L. Wong, C. M. Schowalter, T. J. Jensen, F. R. Fronczek, I. M. Warner and R. M. Strongin, *Proc. Natl. Acad. Sci.*, 2008, **105**, 8829-8834.
- X. Tan, S. Luo, L. Long, Y. Wang, D. Wang, S. Fang, Q. Ouyang, Y. Su, T. Cheng and C. Shi, *Adv. Mater.*, 2017, **29**, 1704196.
- D. Shcherbo, I. I. Shemiakina, A. V. Ryabova, K. E. Luker, B. T. Schmidt, E. A. Souslova, T. V. Gorodnicheva, L. Strukova, K. M. Shidlovskiy, O. V. Britanova, A. G. Zharitsky, K. A. Lukyanov, V. B. Loschenov, G. D. Luker and D. M. Chudakov, *Nat. Methods*, 2010, **7**, 827-830.
- A. M. Derfus, W. C. W. Chan and S. N. Bhatia, *Nano Lett.*, 2004, **4**, 11-18.
- G. Xu, Y. Tang and W. Lin, *New J. Chem.*, 2018, **42**, 12615-12620.
- J. O. Escobedo, O. Rusin, S. Lim and R. M. Strongin, *Curr. Opin. Chem. Biol.*, 2010, **14**, 64-70.
- S. Luo, E. Zhang, Y. Su, T. Cheng and C. Shi, *Biomaterials*, 2011, **32**, 7127-7138.
- L. Yuan, W. Lin and H. Chen, *Biomaterials*, 2013, **34**, 9566-9571.
- C.-h. Liu, F.-p. Qi, F.-b. Wen, L.-p. Long, A.-j. Liu and R.-h. Yang, *Methods Appl. Fluoresc.*, 2018, **6**, 024001.
- T. D. Martins, M. L. Pacheco, R. E. Boto, P. Almeida, J. P. S. Farinha and L. V. Reis, *Dye Pigment*, 2017, **147**, 120-129.
- M. Mitsunaga, M. Ogawa, N. Kosaka, L. T. Rosenblum, P. L. Choyke and H. Kobayashi, *Nat. Med.*, 2011, **17**, 1685-1692.
- J. M. Ball, N. K. S. Davis, J. D. Wilkinson, J. Kirkpatrick, J. Teuscher, R. Gunning, H. L. Anderson and H. J. Snaithe, *Rsc Adv.*, 2012, **2**, 6846-6853.
- L. H. Hutter, B. J. Mueller, K. Koren, S. M. Borisov and I. Klimant, *J. Mater. Chem. C*, 2014, **2**, 7589-7598.
- A. B. Descalzo, H.-J. Xu, Z.-L. Xue, K. Hoffmann, Z. Shen, M. G. Weller, X.-Z. You and K. Rurack, *Org. Lett.*, 2008, **10**, 1581-1584.
- L. Zhang, L.-Y. Zou, J.-F. Guo, D. Wang and A.-M. Ren, *New J. Chem.*, 2015, **39**, 8342-8355.
- J. V. Frangioni, *Curr. Opin. Chem. Biol.*, 2003, **7**, 626-634.
- C. Jiao and J. Wu, *Curr. Org. Chem.*, 2010, **14**, 2145-2168.
- F. J. M. Hoeben, P. Jonkheijm, E. W. Meijer and A. P. H. J. Schenning, *Chem. Rev.*, 2005, **105**, 1491-1546.
- W. Z. Yuan, P. Lu, S. Chen, J. W. Y. Lam, Z. Wang, Y. Liu, H. S. Kwok, Y. Ma and B. Z. Tang, *Adv. Mater.*, 2010, **22**, 2159-2163.
- Z. Zhao, B. He and B. Z. Tang, *Chem. Sci.*, 2015, **6**, 5347-5365.
- D. Wang, H. Su, R. T. K. Kwok, X. Hu, H. Zou, Q. Luo, M. M. S. Lee, W. Xu, J. W. Y. Lam and B. Z. Tang, *Chem. Sci.*, 2018, **9**, 3685-3693.
- S. Mo, Q. Meng, S. Wan, Z. Su, H. Yan, B. Z. Tang and M. Yin, *Adv. Funct. Mater.*, 2017, **27**, 1701210.

- 1  
2  
3  
4  
5  
6  
7  
8  
9  
10  
11  
12  
13  
14  
15  
16  
17  
18  
19  
20  
21  
22  
23  
24  
25  
26  
27  
28  
29  
30  
31  
32  
33  
34  
35  
36  
37  
38  
39  
40  
41  
42  
43  
44  
45  
46  
47  
48  
49  
50  
51  
52  
53  
54  
55  
56  
57  
58  
59  
60
- 30 W. Liu, X. Zhang, L. Zhou, L. Shang and Z. Su, *J. Colloid Interface Sci.*, 2019, **536**, 160-170.
- 31 Z. Wu, S. Mo, L. Tan, B. Fang, Z. Su, Y. Zhang and M. Yin, *Small*, 2018, **14**, 1802524.
- 32 Z. Miao, Z. Gao, R. Chen, X. Yu, Z. Su and G. Wei, *Curr. Med. Chem.*, 2018, **25**, 1920-1944.
- 33 M. Rujimethabhas and P. Wilairat, *J. Chem. Educ.*, 1978, **55**, 342-342.
- 34 K. Kalyanasundaram and J. K. Thomas, *J. Am. Chem. Soc.*, 1977, **99**, 2039-2044.
- 35 M. Irie and M. Mohri, *J. Org. Chem.*, 1988, **53**, 803-808.
- 36 H. Tian and S. Yang, *Chem. Soc. Rev.*, 2004, **33**, 85-97.
- 37 K. Namba and S. Suzuki, *Chem. Lett.*, 1975, DOI: 10.1246/cl.1975.947, 947-950.
- 38 Y. Hong, J. W. Y. Lam and B. Z. Tang, *Chem. Soc. Rev.*, 2011, **40**, 5361-5388.
- 39 J. D. Luo, Z. L. Xie, J. W. Y. Lam, L. Cheng, H. Y. Chen, C. F. Qiu, H. S. Kwok, X. W. Zhan, Y. Q. Liu, D. B. Zhu and B. Z. Tang, *Chem. Commun.*, 2001, DOI: 10.1039/b105159h, 1740-1741.
- 40 D. R. Larson, W. R. Zipfel, R. M. Williams, S. W. Clark, M. P. Bruchez, F. W. Wise and W. W. Webb, *Science*, 2003, **300**, 1434-1436.
- 41 X. Li, X. Gao, W. Shi and H. Ma, *Chem. Rev.*, 2014, **114**, 590-659.
- 42 L. Zhao, X. Cheng, Y. Ding, Y. Yan and J. Huang, *Soft Matter*, 2012, **8**, 10472-10478.
- 43 S. Liu, L. Zhao, Y. Yan and J. Huang, *Soft Matter*, 2015, **11**, 2752-2757.
- 44 M. Gao, L. Wang, J. Chen, S. Li, G. Lu, L. Wang, Y. Wang, L. Ren, A. Qin and B. Z. Tang, *Chem. Eur. J.*, 2016, **22**, 5107-5112.
- 45 D. Yu, Q. Zhang, C. Wu, Y. Wang, L. Peng, D. Zhang, Z. Li and Y. Wang, *J. Phys. Chem. B*, 2010, **114**, 8934-8940.
- 46 J. Cao, L. Ding, W. Hu, X. Chen, X. Chen and Y. Fang, *Langmuir*, 2014, **30**, 15364-15372.
- 47 Y. Cao, L. Ding, W. Hu, J. Peng and Y. Fang, *J. Mater. Chem. A*, 2014, **2**, 18488-18496.
- 48 J. Cao, L. Ding, Y. Zhang, S. Wang and Y. Fang, *J. Photochem. Photobiol. A: Chem.*, 2016, **314**, 66-74.
- 49 L. Peng, G. Zhang, D. Zhang, J. Xiang, R. Zhao, Y. Wang and D. Zhu, *Org. Lett.*, 2009, **11**, 4014-4017.
- 50 X. Shen, G. Zhang and D. Zhang, *Org. Lett.*, 2012, **14**, 1744-1747.
- 51 L. Peng, G. Zhang, D. Zhang, Y. Wang and D. Zhu, *Analyst*, 2010, **135**, 1779-1784.
- 52 J. M. Lim, P. Kim, M.-C. Yoon, J. Sung, V. Dehm, Z. Chen, F. Würthner and D. Kim, *Chem. Sci.*, 2013, **4**, 388-397.
- 53 M. P. Aldred, G.-F. Zhang, C. Li, G. Chen, T. Chen and M.-Q. Zhu, *J. Mater. Chem. C*, 2013, **1**, 6709-6718.
- 54 N.-H. Xie, C. Li, J.-X. Liu, W.-L. Gong, B. Z. Tang, G. Li and M.-Q. Zhu, *Chem. Commun.*, 2016, **52**, 5808-5811.
- 55 Q. Zhao, K. Li, S. Chen, A. Qin, D. Ding, S. Zhang, Y. Liu, B. Liu, J. Z. Sun and B. Z. Tang, *J. Mater. Chem.*, 2012, **22**, 15128-15135.
- 56 Q. Zhao, S. Zhang, Y. Liu, J. Mei, S. Chen, P. Lu, A. Qin, Y. Ma, J. Z. Sun and B. Z. Tang, *J. Mater. Chem.*, 2012, **22**, 7387-7394.
- 57 Q. Zhao, X. A. Zhang, Q. Wei, J. Wang, X. Y. Shen, A. Qin, J. Z. Sun and B. Z. Tang, *Chem. Commun.*, 2012, **48**, 11671-11673.
- 58 D.-Y. Wang, C. Wang and M. Uchiyama, *J. Am. Chem. Soc.*, 2015, **137**, 10488-10491.
- 59 R. Sauer, A. Turshatov, S. Balushev and K. Landfester, *Macromolecules*, 2012, **45**, 3787-3796.
- 60 D. Yu, F. Huang and H. Xu, *Anal. Methods*, 2012, **4**, 47-49.
- 61 L. Peng, Y.-N. Chen, Y. Qiang Dong, C. He and H. Wang, *J. Mater. Chem. C*, 2017, **5**, 557-565.
- 62 B. Song, G. Wu, Z. Wang, X. Zhang, M. Smet and W. Dehaen, *Langmuir*, 2009, **25**, 13306-13310. DOI: 10.1039/C9NJ01184F
- 63 H. Wang, D. Wang, Q. Wang, X. Li and C. A. Schalley, *Org. Biomol. Chem.*, 2010, **8**, 1017-1026.
- 64 S. Guha, S. Lohar, A. Banerjee, A. Sahana, I. Hauli, S. K. Mukherjee, J. Sanmartin Matalobos and D. Das, *Talanta*, 2012, **91**, 18-25.
- 65 A. Sarbu, L. Biniek, J. M. Guenet, P. J. Mesini and M. Brinkmann, *J. Mater. Chem. C*, 2015, **3**, 1235-1242.

## TOC

Highly emissive near-infrared nano-emitters formed by co-assembly of ionic amphiphiles were applicable in cell imaging.

